

Probing torsion field with Einstein-Cartan gravity at the HL-LHC: an angular distribution case study

S. Elgammal*

Centre for Theoretical Physics, The British University in Egypt,
P.O. Box 43, El Sherouk City, Cairo 11837, Egypt.

(Dated: January 29, 2026)

This analysis utilizes simulated data privately generated based on the High Luminosity Large Hadron Collider (HL-LHC) configuration to investigate the angular distribution of high-mass dimuon pairs produced during the foreseen proton-proton collisions at a center-of-mass energy of 14 TeV. The study focuses on the $\cos\theta_{CS}$ variable, which is defined in the Collins-Soper frame. In the Standard Model, the production of high-mass dimuon pairs is primarily governed by the Drell-Yan process, which demonstrates a significant forward-backward asymmetry. However, scenarios beyond the Standard Model suggest different shapes for the $\cos\theta_{CS}$ distribution. By observing excess events not predicted by the Standard Model, the angular distribution can help differentiate among these alternative models. Furthermore, we used a simplified Einstein-Cartan gravity model to analyze the simulated data. This analysis established upper limits at the 95% confidence level regarding the masses of various particles within the model, including a spin-2 dark neutral gauge boson and the torsion field.

I. INTRODUCTION

One of the methods for detecting physics beyond the Standard Model (SM) [1] at the Large Hadron Collider (LHC) involves observing changes in the dilepton mass spectrum at high mass. Such changes might appear as a new peak, as anticipated by heavy neutral gauge boson models, like Z' [2], or by Randall-Sundrum models [3]. Alternatively, the spectrum could display a broad distortion, which might indicate the presence of Contact Interactions [4, 5] or models such as ADD [6].

The CMS collaboration has focused extensively on these signatures, particularly concerning Z' and Contact Interaction models [7]. Another model, known as Mono- Z' [8, 9], predicts the production of dark matter in conjunction with Z' .

Previous studies performed by the CMS [10] and ATLAS [11] collaborations utilized the angular distributions of Drell-Yan charged lepton pairs around the Z boson mass peak to measure the forward-backward asymmetry (A_{FB}). Both studies analyzed the complete LHC Run 1 data, which included an integrated luminosity of 19.7 fb^{-1} for CMS and 20.3 fb^{-1} for ATLAS, based on proton-proton collisions at a center of mass energy of 8 TeV (\sqrt{s}). The measurements of A_{FB} were found to be consistent with predictions from the Standard Model.

Moreover, the forward-backward asymmetry of high-mass dileptons (with $M_{ll} > 170$ GeV) has been measured using the CMS detector at $\sqrt{s} = 13$ TeV, with an integrated luminosity of 138 fb^{-1} . This analysis concluded that no statistically significant deviations from the Standard Model predictions were observed [12].

In the current analysis, we studied the angular distributions of the dimuon channel in mass bins above the Z -

boson mass peak, utilizing Monte Carlo simulated data from the CMS experiment for the HL-LHC [13], which has an integrated luminosity of 3000 fb^{-1} at a center-of-mass energy of $\sqrt{s} = 14$ TeV [14]. To interpret the simulated data, we employed a simplified model [15] based on Einstein-Cartan (EC) gravity [16–21]. This model is for the dark neutral gauge boson (A') production alongside dark matter (DM) at the HL-LHC. Many cosmological observations, based on recent observations by [22–24], support the existence of dark matter. These observations suggest that dark matter is non-decaying, and weakly interacting massive particles [25, 26].

Several searches for dark matter (DM) have been conducted using data collected from the CMS and ATLAS experiments during RUN II [27, 28]. These searches focus on the production of a visible object, referred to as "X," which recoils against the significant missing transverse energy resulting from dark matter particles. This creates a signature of $(X + E_T^{\text{miss}})$ in the detector [29]. The visible particle "X" could be a Standard Model (SM) particle, such as W or Z bosons, jets [30–33], a photon [34, 35], or even the SM Higgs boson [36–38].

Additionally, we provide a statistical interpretation of the results. The simulated data for the signal and the standard model backgrounds were produced privately.

The analysis is structured as follows: A theoretical model based on Einstein-Cartan gravity is discussed in section II. Section III introduces the Collins-Soper frame and the variable $\cos\theta_{CS}$ as it pertains to Drell-Yan events, including the quark direction ambiguity. A brief overview of the HL-LHC project is provided in section IV. Section V covers the Monte Carlo production of signal samples used in the analysis, followed by an exploration of significant SM background processes. The analysis strategy and event selection criteria are detailed in section VI. In section VII, we present results based on angular distribution ($\cos\theta_{CS}$) and statistical interpretation. Finally, a summary is offered in section VIII.

* sherif.elgammal@bue.edu.eg

II. THE THEORETICAL SIGNAL MODEL

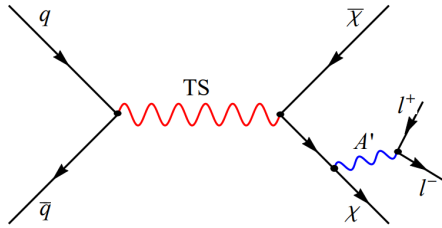


Figure 1 Feynman diagram for the simplified model based on Einstein-Cartan gravity; for the production of dark gauge boson (A') in association to dark matter (χ) pair [15].

The simplified model analyzed is based on Einstein-Cartan gravity, which discusses dark matter production from proton-proton collisions at the HL-LHC, alongside a new neutral dark gauge boson A' [15].

This dark gauge boson (A'_μ) can result from the pair annihilation of quarks $q\bar{q}$ mediated by the heavy torsion field (S_ρ), leading to the generation of two dark matter particles (χ). The dark matter is sufficiently heavy to decay into an A'_μ and another dark matter particle (χ), as illustrated in figure 1.

The interaction terms, in the effective Lagrangian, between the torsion field and Dirac fermion (ψ), is given by [15]

$$\bar{\psi}i\gamma^\mu(\partial_\mu + ig_\eta\gamma^5S_\mu + \dots)\psi.$$

According to the previous equation, the torsion field interacts with both the SM and hidden fermions through its axial-vector component, characterized by a universal coupling constant of g_η . In dynamical torsion theories, such as the one discussed in [15], the classical coupling constant g_η holds a fixed value of $\frac{1}{8}$ (0.125). This specific value emerges from the underlying structure of the theory and how torsion interacts with fermions.

The effective Lagrangian term for the torsion field coupling to dark matter and the interaction between the dark gauge boson (A'_μ) and dark matter is given by [15].

$$\bar{\chi}(i\gamma^\mu D_\mu - M_\chi)\chi.$$

The expression for the covariant derivative is $D_\mu = \partial_\mu + ig_\eta\gamma^5S_\mu + ig_D A'_\mu$. The dark matter mass is denoted by M_χ , and the dark gauge boson coupling to dark matter is $g_D = 1.0$ as suggested from the LHC Dark Matter Working Group [41].

The neutral dark gauge boson (A') decays into SM fermion pairs, specifically focusing on the muonic decay $A' \rightarrow \mu^+\mu^-$, which has the highest branching ratio under certain mass conditions outlined in table I. The model includes several free parameters: the masses of the torsion field (M_{TS}), dark gauge boson ($M_{A'}$), and dark matter (M_χ).

Previous indirect searches for dark matter have shown a promising chance of detecting dark matter with masses ranging from 100 to 10,000 GeV [39, 40]. For our analysis, we have chosen the dark matter mass to be $M_\chi = 500$ GeV. In this context, we have fixed the coupling constants at $g_\eta = 0.125$ and $g_D = 1.0$. Meanwhile, the parameters M_{TS} and $M_{A'}$ are treated as free variables, and their specific values are detailed in Table I.

The signature of this process features a pair of opposite-sign muons from the decay of A' , along with significant missing transverse energy due to stable dark matter χ . We focus on the topology $\mu^+\mu^- + E_T^{miss}$, which offers a clean signal against SM backgrounds, especially since the CMS detector is optimized for this channel.

III. THE COLLINS-SOPER FRAME

In hadron colliders, two partons can collide to produce a lepton pair ($\ell^+\ell^-$) through the Drell-Yan process ($q\bar{q} \rightarrow \gamma^*/Z \rightarrow \ell^+\ell^-$), which is the only tree-level process in the Standard Model for this outcome. In the current analysis, we analyze the angular distribution of these pairs in the Collins-Soper (CS) frame [42], which reduces distortions from the transverse momenta of the incoming partons. However, accurately measuring the angle θ between the negative lepton and one of the partons is challenging if either parton has non-zero transverse momentum, and the direction of the quark is not easily determined in $q\bar{q}$ annihilation.

We adopt the Collins-Soper frame to explore the angular distribution of lepton pairs effectively. In this frame, the angle θ_{CS} is defined as the angle between the momentum of the negative lepton and the z-axis. By using this frame, we aim to reduce the uncertainties that arise from the unknown transverse momentum of the incoming quarks.

To determine the orientation of the Collins-Soper frame, we rely on the sign of the longitudinal boost of the dilepton system. We can compute the angle $\cos\theta_{CS}$ from quantities that we measure in the lab frame, as explained in [10].

$$\cos\theta_{CS} = \frac{|Q_z|}{Q_z} \frac{2(P_1^+P_2^- - P_1^-P_2^+)}{\sqrt{Q^2(Q^2 + Q_T^2)}}. \quad (1)$$

The symbols Q , Q_T , and Q_z stand for the four-momentum, the transverse momentum, and the longitudinal momentum of the dimuon system, respectively. Similarly, P_1 (P_2) represents the four-momentum of μ^- (μ^+), and E_i denotes the energy of the muon. In addition, P_i^\pm is defined as $(E_i \pm P_{z,i})/\sqrt{2}$.

IV. THE HL-LHC PROJECT

The LHC has undergone several upgrades, including Runs I, II, and III, proving its value. The upcoming

Table I The parameters of the simplified model drawing on the principles of Einstein-Cartan gravity, all while considering a specific mass assumption [15].

Parameters	Description	optimized value
M_{TS}	Mass of torsion field (TS)	[1250, ..., 7000] GeV
$M_{A'}$	Mass of dark gauge boson (A')	[200, ..., 600] GeV
M_χ	Mass of dark matter (χ)	500 GeV [39, 40]
g_D	Coupling of dark gauge boson to dark matter	1.0 [41]
g_η	Coupling of torsion field to Dirac fermions	0.125 [15]
Mass assumption	$M_{A'} < 2M_\chi$ [15]	

HL-LHC upgrade will enhance the center of mass energy ($\sqrt{s} = 14$ TeV) and increase proton collisions for better data. This will involve installing new equipment over 1.2 km of the 27 km LHC [13].

The CMS detector at CERN’s LHC searches for new physics using a complex structure and various angular measurements: the polar angle (θ), azimuthal angle (ϕ), and pseudo-rapidity (η). The coordinate system has the z-axis along the beam axis, the x-axis toward the LHC center, and the y-axis upwards. The ϕ measurement occurs in the x-y transverse plane, while θ is along the x-axis. The direction of the collision products is described by η , defined as $\eta = -\ln[\tan(\theta/2)]$ [43, 44].

V. SIMULATED SAMPLES AND BACKGROUND ESTIMATION

A. Monte Carlo simulation of the model signals

We generated the events of the signal model using MadGraph5_aMC@NLO v3.5.0 [45]. The cross-section was calculated at NLO, and Pythia 8 [46] was employed for the hadronization process, and DELPHES [47] for a fast detector simulation of HL-LHC. We analyzed the production cross-section for various mass combinations of the dark gauge boson ($M_{A'}$) and torsion field (M_{TS}), assuming $g_\eta = 0.125$, $g_D = 1.0$, and a dark matter mass of $M_\chi = 500$ GeV. The Monte Carlo signal samples used in this analysis and their corresponding cross-sections are listed in Table II.

B. Monte Carlo simulation of the SM backgrounds

The SM background processes yielding muon pairs in the signal region are Drell-Yan ($DY \rightarrow \mu^+\mu^-$), the production of top quark pairs ($t\bar{t} \rightarrow \mu^+\mu^- + 2b + 2\nu$), $tW \rightarrow \mu^+\mu^- + 2\nu + b$, and production of diboson ($W^+W^- \rightarrow \mu^+\mu^- + 2\nu$, $ZZ \rightarrow \mu^+\mu^- + 2\nu$ and $W^\pm Z \rightarrow \mu^\pm\mu^+\mu^- + \nu$).

Another source of background is the jet background, which arises from misidentifying jets as muons, particularly from W+jets and QCD multijet processes. This background is typically estimated using a data-driven method, as detailed in [48]. However, it is irrelevant to

our study, which relies exclusively on MC simulations, and no W+jets events pass our analysis pre-selection. In addition, further cuts are implemented, detailed in section VII, which rely on variables such as ($\Delta\phi$ (lepton, MET), MET, etc.). These cuts are often used to strongly suppress the QCD events in which MET aligns with a mismeasured jet, as discussed in ref. [49].

The SM processes were generated using MadGraph5_aMC@NLO with Pythia 8 for parton showering and DELPHES for fast detector simulation of the HL-LHC. They were derived from 14 TeV proton-proton collisions, with muon $p_T > 10$ GeV and $|\eta| < 3$.

All Monte Carlo samples used in this analysis and their cross sections were computed in next-to-leading order. Signal samples and SM background contributions were estimated from the simulations, normalized to their corresponding cross-section, and an integrated luminosity of 3000 fb^{-1} .

VI. EVENT SELECTION

The event selection for the analysis aims to reconstruct a final state with two high transverse momentum (p_T) muons and missing transverse energy, indicative of a dark matter candidate.

The pre-selection criteria for each muon include: $p_T^\mu > 30$ GeV, $|\eta^\mu| < 2.5$ rad, and $\text{IsolationVarRhoCorr} < 0.1$.

The isolation cut in DELPHES requires that the scalar p_T sum of all muon tracks within a cone of $\Delta R = 0.5$ around the muon does not exceed 10% of the muon’s p_T , adjusted for pileup effects.

Events are selected with two oppositely charged muons, and the dimuon invariant mass must be greater than 60 GeV to search for high-mass resonances. These cuts are summarized in Table III. We present the distribution of $\cos\theta_{CS}$ for a resonant model based on Einstein-Cartan gravity in Figure 2. The model assumes a dark boson (A') mass of 200 GeV, and we compare it with Drell-Yan events. All events meet the pre-selection criteria outlined in Table III and have a reconstructed invariant mass ranging from 160 to 240 GeV. The results are illustrated with black open circles representing the model signal and blue closed circles for the Drell-Yan events,

Table II The simplified model (based on Einstein Cartan gravity) cross-section measurements times branching ratios (in pb) calculated for different sets of the masses $M_{A'}$ (in GeV), and M_{TS} (in GeV), for the mass assumption given in table I, with dark matter mass ($M_\chi = 500$ GeV), the following couplings constants $g_\eta = 0.125$, $g_D = 1.0$ and at $\sqrt{s} = 14$ TeV.

M_{TS}	1250	1500	1750	1800	1970	2000	3000	4000	5000	6000	7000
$M_{A'}$	200	300	400	500	600	700	800	900	1000	1100	1200
200	7.1×10^{-5}	10.0×10^{-4}	26.7×10^{-4}	28.2×10^{-4}	30.6×10^{-4}	30.8×10^{-4}	15.8×10^{-4}	4.7×10^{-4}	1.2×10^{-4}	2.6×10^{-5}	5.1×10^{-6}
300	1.3×10^{-5}	6.6×10^{-4}	18.0×10^{-4}	19.7×10^{-4}	23.7×10^{-4}	24.0×10^{-4}	15.1×10^{-4}	4.8×10^{-4}	1.3×10^{-4}	2.8×10^{-5}	5.6×10^{-6}
400	9.8×10^{-7}	1.7×10^{-4}	10.8×10^{-4}	12.4×10^{-4}	16.9×10^{-4}	17.4×10^{-4}	13.7×10^{-4}	4.7×10^{-4}	1.3×10^{-4}	2.9×10^{-5}	6.0×10^{-6}
500	7.5×10^{-7}	9.7×10^{-7}	2.7×10^{-4}	3.5×10^{-4}	7.7×10^{-4}	7.9×10^{-4}	12.3×10^{-4}	4.6×10^{-4}	1.3×10^{-4}	3.0×10^{-5}	6.3×10^{-6}
600	6.1×10^{-7}	7.7×10^{-7}	1.8×10^{-4}	2.9×10^{-4}	6.4×10^{-4}	7.0×10^{-4}	10.1×10^{-4}	4.1×10^{-4}	1.2×10^{-4}	2.8×10^{-5}	6.0×10^{-6}

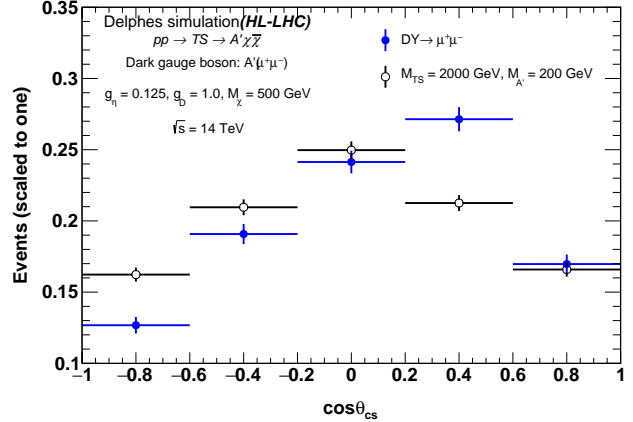


Figure 2 Normalized distributions of $\cos\theta_{CS}$ for one resonant model based on Einstein-Cartan gravity generated with a mass of A' equal to 200 GeV and Drell-Yan events at $\sqrt{s} = 14$ TeV. All events must pass the pre-selection listed in table III and have a reconstructed invariant mass in the 160 - 240 GeV range. All histograms are normalized to unity to highlight qualitative features.

Table III Summary of cut-based event selections used in the analysis.

Pre-selection	Final selection
$p_T^\mu > 30$ GeV $ \eta^\mu < 2.5$ rad $\sum_i p_T^i / p_T^\mu < 0.1$ $M_{\mu^+\mu^-} > 60$ GeV	$p_T^\mu > 30$ GeV $ \eta^\mu < 2.5$ rad $\sum_i p_T^i / p_T^\mu < 0.1$ $M_{A'} - 40 < M_{\mu^+\mu^-} < M_{A'} + 40$ $\Delta\phi_{\mu^+\mu^-, E_T^{\text{miss}}} > 2.5$ rad $ E_T^{\mu^+\mu^-} - E_T^{\text{miss}} / E_T^{\mu^+\mu^-} < 0.4$ $\cos(\text{angle}_{3D}) < -0.75$ $N_{\text{jets}} < 1$

normalized to unity. We observe a clear distinction between the simplified model and the Drell-Yan events. The signal shape exhibits a typical characteristic of a spin-2 boson, displaying a symmetric distribution around zero. This distribution aligns with the findings from the study conducted in [50].

The graphs in figure 3 show the distribution of $\cos\theta_{CS}$ across different mass bins: $160 < M_{\mu^+\mu^-} < 240$ GeV 3(a), $260 < M_{\mu^+\mu^-} < 340$ GeV 3(b), $360 < M_{\mu^+\mu^-} < 440$ GeV 3(c), $460 < M_{\mu^+\mu^-} < 540$ GeV 3(d), and $560 < M_{\mu^+\mu^-} < 640$ GeV 3(e). The histograms in green, blue, and gray represent Drell-Yan, $t\bar{t} + tW$, and vector boson pair backgrounds, respectively, stacked together, with the red dotted line indicating the Einstein-Cartan signal for the dark neutral gauge boson A' , with $M_\chi = 500$ GeV and $M_{TS} = 2000$ GeV.

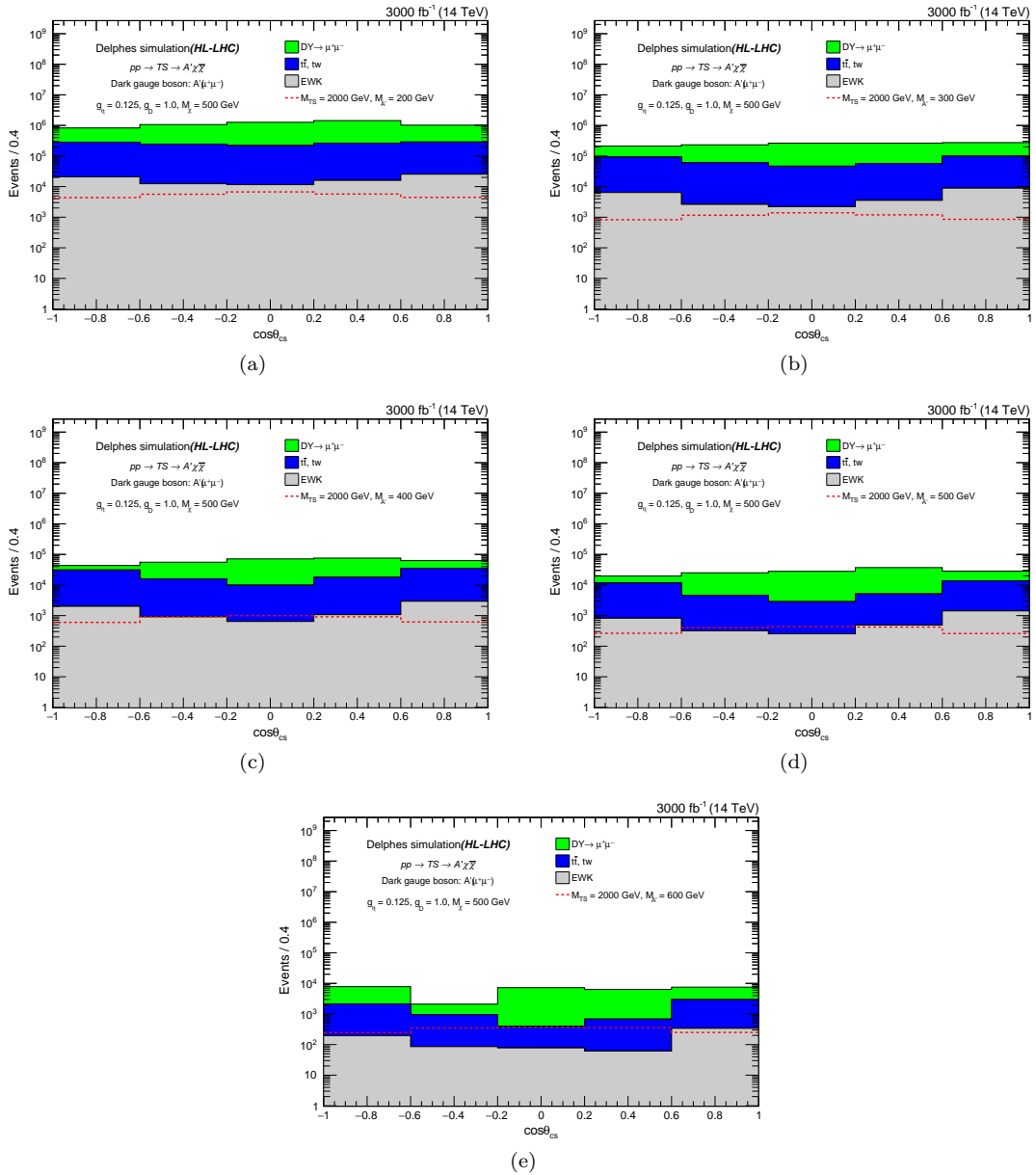


Figure 3 Distributions of $\cos\theta_{CS}$ are illustrated, for events passing pre-selection listed in table III, for the standard model expectations (histograms) for several dimuon mass windows: $160 < M_{\mu^+\mu^-} < 240$ GeV 3(a), $260 < M_{\mu^+\mu^-} < 340$ GeV 3(b), $360 < M_{\mu^+\mu^-} < 440$ GeV 3(c), $460 < M_{\mu^+\mu^-} < 540$ GeV 3(d), and $560 < M_{\mu^+\mu^-} < 640$ GeV 3(e). The signal presentation of the model corresponding to the Einstein-Cartan gravity with the value of $M_{A'}$ runs from 200 to 600 GeV is superimposed.

VII. RESULTS

After applying the pre-selection cuts presented in Table III, the Einstein-Cartan signal events were fully im-peded in the SM background; thus, a tighter selection has been optimized to distinguish the model signals from the SM backgrounds.

The tight selection is based on five variables:

1. We calculate the azimuthal angle difference

$\Delta\phi_{\mu^+\mu^-, \vec{E}_T^{\text{miss}}}$, which represents the difference between the azimuthal angles of the dimuon and the missing transverse energy ($|\phi^{\mu^+\mu^-} - \phi^{\text{miss}}|$). This value must be greater than 2.5 radians.

2. We evaluate the relative difference between the transverse energy of the dimuon ($E_T^{\mu^+\mu^-}$) and the missing transverse energy (E_T^{miss}). This difference is set to be less than 0.4, defined by the condition $|E_T^{\mu^+\mu^-} - E_T^{\text{miss}}|/E_T^{\mu^+\mu^-} < 0.4$.

3. We impose a constraint on the cosine of the 3D angle between the missing energy vector and the dimuon system vector to ensure they are oriented back-to-back, requiring that $\cos(\text{angle}_{3D}) < -0.75$.

4. The number of jets (N_{jets}) with $p_T^j > 20$ GeV and $|\eta^j| < 2.5$ should be less than 1.

Lastly, we limit the invariant mass of the dimuon to a range centered around the mass of the neutral gauge boson A' . Specifically, we require that $M_{A'} - 40 < M_{\mu^+ \mu^-} < M_{A'} + 40$.

In Figure 4, we present the distributions of several variables for dimuon events, where each muon meets the pre-selection criteria outlined in Section VI. These variables include $\Delta\phi_{\mu^+ \mu^-, \vec{E}_T^{\text{miss}}}$ 4(a), the normalized difference $|E_T^{\mu^+ \mu^-} - E_T^{\text{miss}}|/E_T^{\mu^+ \mu^-}$ 4(b), $\cos(\text{angle}_{3D})$ 4(c), and the number of jets (N_{jets}) 4(d). The dotted and solid black histograms illustrate two signal scenarios from the Einstein-Cartan gravity model, corresponding to $M_{A'}$ values of 200 GeV and 500 GeV. These scenarios feature a dark matter mass of $M_\chi = 500$ GeV and mass of the torsion field $M_{TS} = 2000$ GeV, with coupling constants $g_\eta = 0.125$ and $g_D = 1.0$. Additionally, the Standard Model backgrounds are represented by colored histograms. For clarity, all distributions have been normalized to one, and the vertical dashed lines indicate the selected cut values for each variable.

Table III summarizes the strict selection criteria. By applying tighter cuts, in addition to those specified in the pre-selection, we eliminated the DY and ZZ backgrounds. Furthermore, there was a significant reduction in the contributions from the $t\bar{t}$, tW, WW, and WZ backgrounds.

The figures of merit for optimizing these stringent criteria are represented by plotting the N-1 efficiency for each of the four criteria mentioned earlier. The N-1 efficiency is calculated by dividing the number of events that successfully pass the final selection, as shown in Table III, by the number of events that would pass the final selection if the specific cut being considered were not applied.

In figure 5, we present the distributions of the N-1 efficiencies plotted against the transverse momentum of the leading reconstructed muon (p_T^μ) for the following conditions: $\Delta\phi_{\mu^+ \mu^-, \vec{E}_T^{\text{miss}}} > 2.5$ 5(a), $|E_T^{\mu^+ \mu^-} - E_T^{\text{miss}}|/E_T^{\mu^+ \mu^-} < 0.4$ 5(b), $\cos(\text{angle}_{3D}) < -0.75$ 5(c), and $N_{\text{jets}} < 1$ 5(d). These plots focus on the signal in the EC gravity scenario (indicated by black closed circles), with $M_{TS} = 2000$ GeV, $M_{A'} = 200$ GeV, and coupling constants $g_\eta = 0.125$ and $g_D = 1.0$, alongside standard model (SM) backgrounds marked with open colored markers.

The efficiency plots indicate that implementing these four stringent selection cuts significantly reduces background noise from DY and ZZ processes, while also minimizing contamination from $t\bar{t}$, WW, and WZ events. Furthermore, this approach guarantees that the signal maintains a consistently flat efficiency at high p_T levels

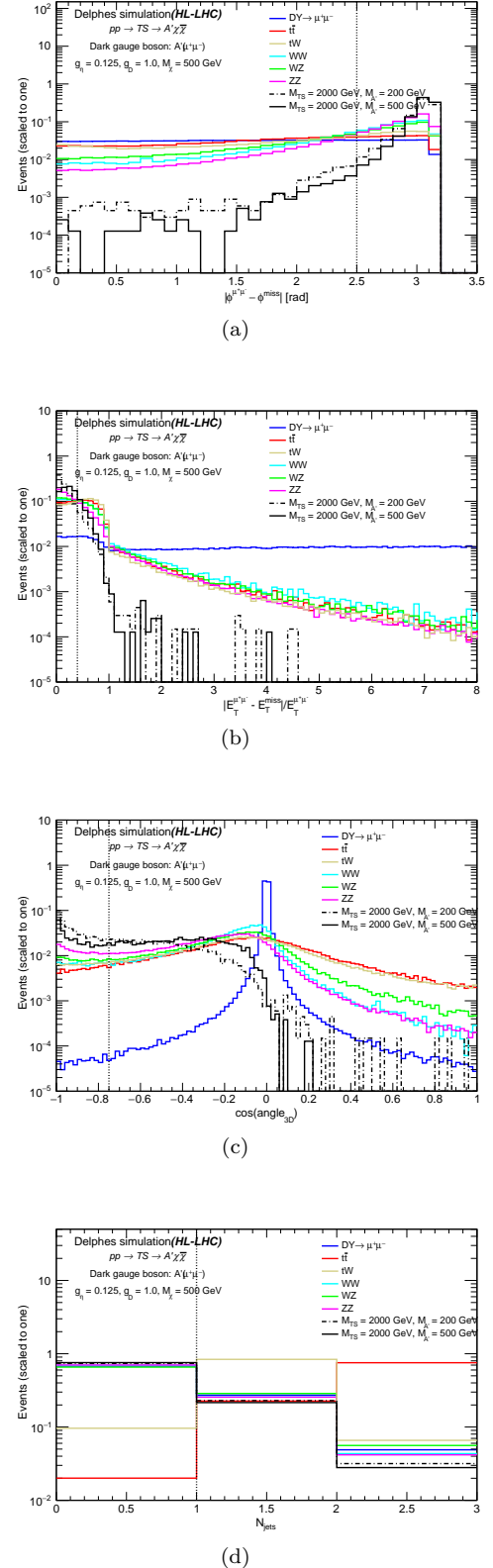


Figure 4 Distributions of $\Delta\phi_{\mu^+ \mu^-, \vec{E}_T^{\text{miss}}}$ 4(a), $|E_T^{\mu^+ \mu^-} - E_T^{\text{miss}}|/E_T^{\mu^+ \mu^-}$ 4(b), $\cos(\text{angle}_{3D})$ 4(c), and the number of jets 4(d) for the signal presentations of the model corresponding to the Einstein-Cartan gravity with $M_{A'} = 200$ and 500 GeV and SM backgrounds, for dimuon events with each muon passing the pre-selection summarized in table III.

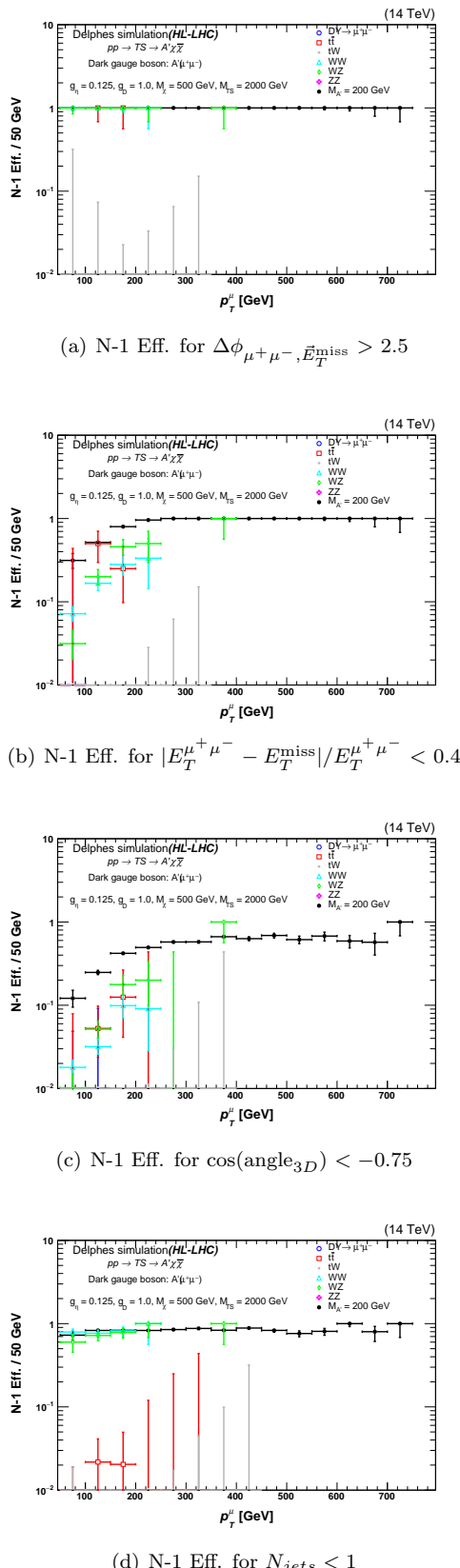


Figure 5 Distributions of the N-1 efficiencies plotted against the transverse momentum of the leading reconstructed muon (p_T^μ) for the 4 analysis cuts. Illustrated for the signal in the EC gravity scenario with $M_{TS} = 2000$ GeV, $M_{A'} = 200$ GeV, and coupling constants $g_\eta = 0.125$ and $g_D = 1.0$ and for the SM backgrounds.

for muons.

The graphs depicted in Figure 6 show the distributions of the $\cos\theta_{CS}$ for events that have passed the event final selection criteria mentioned in Tables III in multiple mass bins: $160 < M_{\mu^+\mu^-} < 240$ GeV 6(a), $260 < M_{\mu^+\mu^-} < 340$ GeV 6(b), $360 < M_{\mu^+\mu^-} < 440$ GeV 6(c), $460 < M_{\mu^+\mu^-} < 540$ GeV 6(d), and $560 < M_{\mu^+\mu^-} < 640$ GeV 6(e). Applying the final cuts mentioned in table III demonstrates that the signal samples are easily distinguishable from the SM backgrounds.

To determine the required values of $M_{A'}$ necessary for observing either a deviation or a potential discovery, we have assessed the signal significance, defined as $S = N_s / \sqrt{N_s + N_b}$, by varying $M_{A'}$. In this formula, N_s represents the number of signal events, while N_b denotes the total number of Standard Model background events that pass the final selection criteria outlined in Table III.

The plots illustrated in Figure 7 display the connection between signal significance (S) and integrated luminosity(L) for a specific dark matter mass scenario, namely $M_\chi = 500$ GeV, using coupling constants of $g_\eta = 0.125$ and $g_D = 1.0$. Plot 7(a) centers on $M_{A'} = 200$ GeV, plot 7(b) focuses on $M_{A'} = 300$ GeV, and plot 7(c) examines $M_{A'} = 400$ GeV, all for events that satisfy the final criteria outlined in Table III. The dashed red line in these plots indicates a significance value of $S = 5$.

In Table IV, we present the calculations for the required luminosity to achieve 5σ significance, denoted as $\mathcal{L}_{5\sigma}^{\text{Req}}$. This is evaluated for two values of M_{TS} , specifically 4000 GeV and 5000 GeV, against the Standard Model background. The analysis spans three different values of $M_{A'}$ and utilizes coupling constants of $g_\eta = 0.125$ and $g_D = 1.0$, with $M_\chi = 500$ GeV, all at a center-of-mass energy of $\sqrt{s} = 14$ TeV.

Table IV The required luminosity to achieve 5σ significance $\mathcal{L}_{5\sigma}^{\text{Req}}$ over the SM background for three $M_{A'}$ values, taking coupling constants $g_\eta = 0.125$ and $g_D = 1.0$, and $M_\chi = 500$ GeV, at $\sqrt{s} = 14$ TeV.

M_{TS} (GeV)	4000	5000
$M_{A'}$ (GeV)	$\mathcal{L}_{5\sigma}^{\text{Req}}$ (fb $^{-1}$)	$\mathcal{L}_{5\sigma}^{\text{Req}}$ (fb $^{-1}$)
200	500	-
300	177	940
400	160	600

A. Statistical interpretation

The shape-based analysis makes effective use of the distributions of $\cos(\theta_{CS})$ as key discriminators. These distributions are especially valuable because they highlight a characteristic signal pattern associated with a typical spin-2 boson, which starkly contrasts the backgrounds outlined by the Standard Model. An ad-hoc flat 10% uncertainty is applied to cover all possible systematic effects.

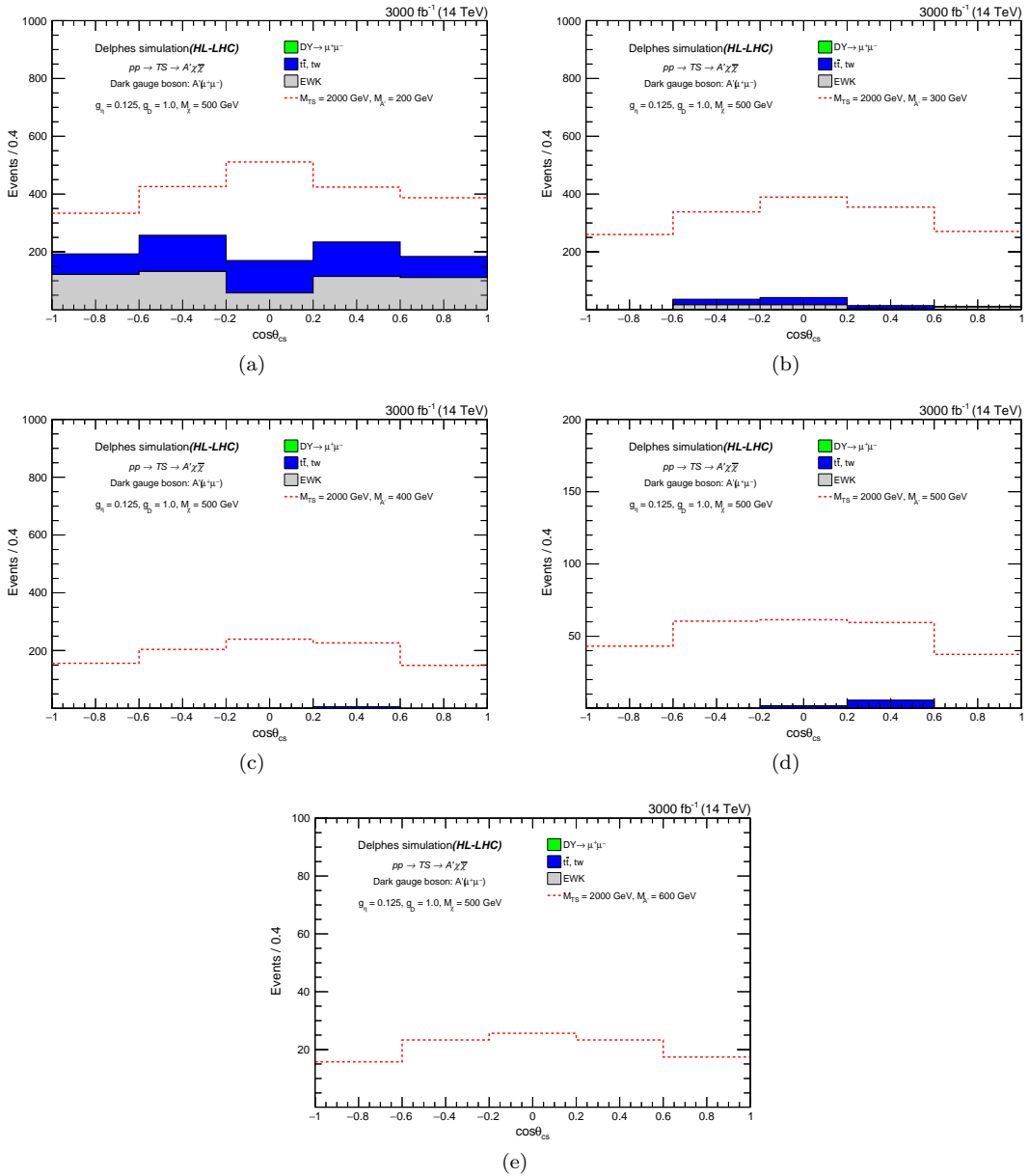


Figure 6 Distributions of $\cos\theta_{CS}$ are illustrated, for events passing final selection listed in table III, for the standard model expectations (histograms) for several dimuon mass windows: $160 < M_{\mu^+\mu^-} < 240 \text{ GeV}$ 6(a), $260 < M_{\mu^+\mu^-} < 340 \text{ GeV}$ 6(b), $360 < M_{\mu^+\mu^-} < 440 \text{ GeV}$ 6(c), $460 < M_{\mu^+\mu^-} < 540 \text{ GeV}$ 6(d), and $560 < M_{\mu^+\mu^-} < 640 \text{ GeV}$ 6(e). The signal presentation of the model corresponding to the Einstein-Cartan gravity with the value of $M_{A'}$ runs from 200 to 600 GeV is superimposed.

We conducted a statistical test using the profile likelihood method to interpret our results statistically. We utilized the modified frequentist construction CLs [51, 52] in the asymptotic approximation [53] to establish exclusion limits on the product of signal cross sections and the branching fraction $\text{Br}(A' \rightarrow \mu\mu)$ at a 95% confidence level.

In Figure 8, we present the expected 95% confidence level (CL) upper limits on the product of the cross-section and the branching ratio as a function of the mediator's

mass (M_{TS}). This analysis is based on Einstein-Cartan gravity and focuses on the muonic decay of the A' . The solid black curves represent this model, which features a fixed dark matter mass of $M_\chi = 500 \text{ GeV}$, coupling parameters $g_\eta = 0.125$ and $g_D = 1.0$ are applied, illustrating a range of A' mass values. Specifically, the values for $M_{A'}$ are set at 200 GeV 8(a), 300 GeV 8(b), 400 GeV 8(c), and 500 GeV 8(d). The vertical red dotted lines in each graph, shown in Figure 8, represent the limit values.

When the mass $M_{A'}$ exceeds 500 GeV, there are not

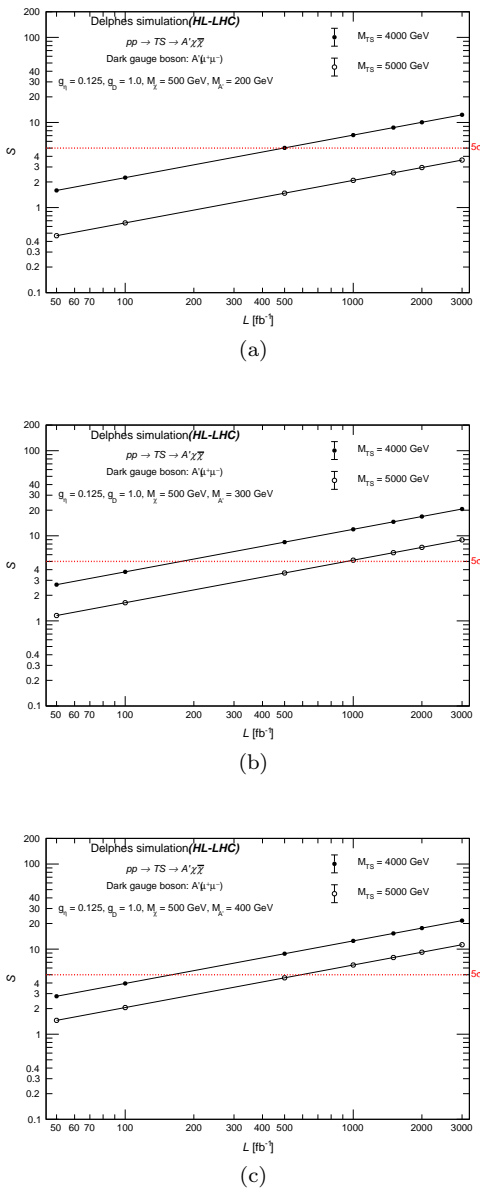


Figure 7 The significance (S) is plotted against the integrated luminosity (L) for events that pass the full set of cuts listed in Table III. This is shown for different tensor scalar masses (M_{TS}): $M_{A'} = 200$ GeV in plot 7(a), 300 GeV in plot 7(b), and 400 GeV in plot 7(c). The model relates to Einstein-Cartan gravity with coupling constants $g_\eta = 0.125$ and $g_D = 1.0$, assuming the dark matter mass is $M_\chi = 500$ GeV. The dashed horizontal red line indicates $S = 5$.

enough standard model background events to conduct a meaningful statistical analysis.

VIII. SUMMARY

One effective strategy for discovering new physics beyond the Standard Model at the Large Hadron Collider involves examining changes in the dilepton mass spectrum, particularly at high masses. Furthermore, analyzing the angular distributions of leptons could distinguish between different models of new physics and assess the spin, parity, and couplings of any potential signals.

Our study focused on the angular distributions of high-mass dimuon pairs in the Collins-Soper frame. The simulated data we worked with were derived from private proton-proton simulated collisions anticipated at the High-Luminosity LHC (HL-LHC), featuring a center-of-mass energy of $\sqrt{s} = 14$ TeV and corresponding to an integrated luminosity of 3000 fb^{-1} .

We concentrated on the $\cos\theta_{CS}$ variable to differentiate between the Standard Model (SM) background and potential new physics beyond it. Our analysis involved comparing the expected distributions of the $\cos\theta_{CS}$ variable for high-mass SM background events with those from a simplified new physics model based on Einstein-Cartan gravity. The resulting signal shape reveals a distinctive feature of a spin-2 A' neutral gauge boson, characterized by a symmetric distribution of $\cos\theta_{CS}$ around zero.

To improve the distinction between signal events and standard model (SM) backgrounds, we implemented strict discrimination cuts that effectively diminished the impacts of Drell-Yan and ZZ backgrounds. This approach also significantly curtailed contributions from $t\bar{t}$, tW , WW , and WZ backgrounds.

With the application of these strong cuts, a mass $M_{A'}$ of 200 GeV allows us to achieve a 5σ discovery at an integrated luminosity of 500 fb^{-1} for the torsion mass ($M_{TS} = 4000$ GeV). In contrast, discovering a torsion mass of $M_{TS} = 5000$ GeV necessitates an integrated luminosity exceeding 2000 fb^{-1} . For a mass $M_{A'}$ of 400 GeV, we can reach a 5σ discovery with an integrated luminosity of 160 fb^{-1} when $M_{TS} = 4000$ GeV. However, if we consider $M_{TS} = 5000$ GeV, a 5σ discovery is achievable with an integrated luminosity of 600 fb^{-1} .

Finally, we have established a 95% confidence level upper limit on certain model-independent parameters within the framework of Einstein-Cartan gravity. With coupling values set at $g_\eta = 0.125$ and $g_D = 1.0$, along with a dark matter mass of $M_\chi = 500$ GeV, we determined specific mass exclusions for the torsion field M_{TS} :

- For an A' boson mass of 200 GeV, the mass values of M_{TS} fall between 1396 and 5545.
- For an A' boson mass of 300 GeV, the corresponding mass values of M_{TS} range from 1402 to 6310.
- For an A' boson mass of 400 GeV, the mass values of M_{TS} span from 1537 to 7026.
- For an A' boson mass of 500 GeV, the mass values of M_{TS} extend from 1677 to 6927.

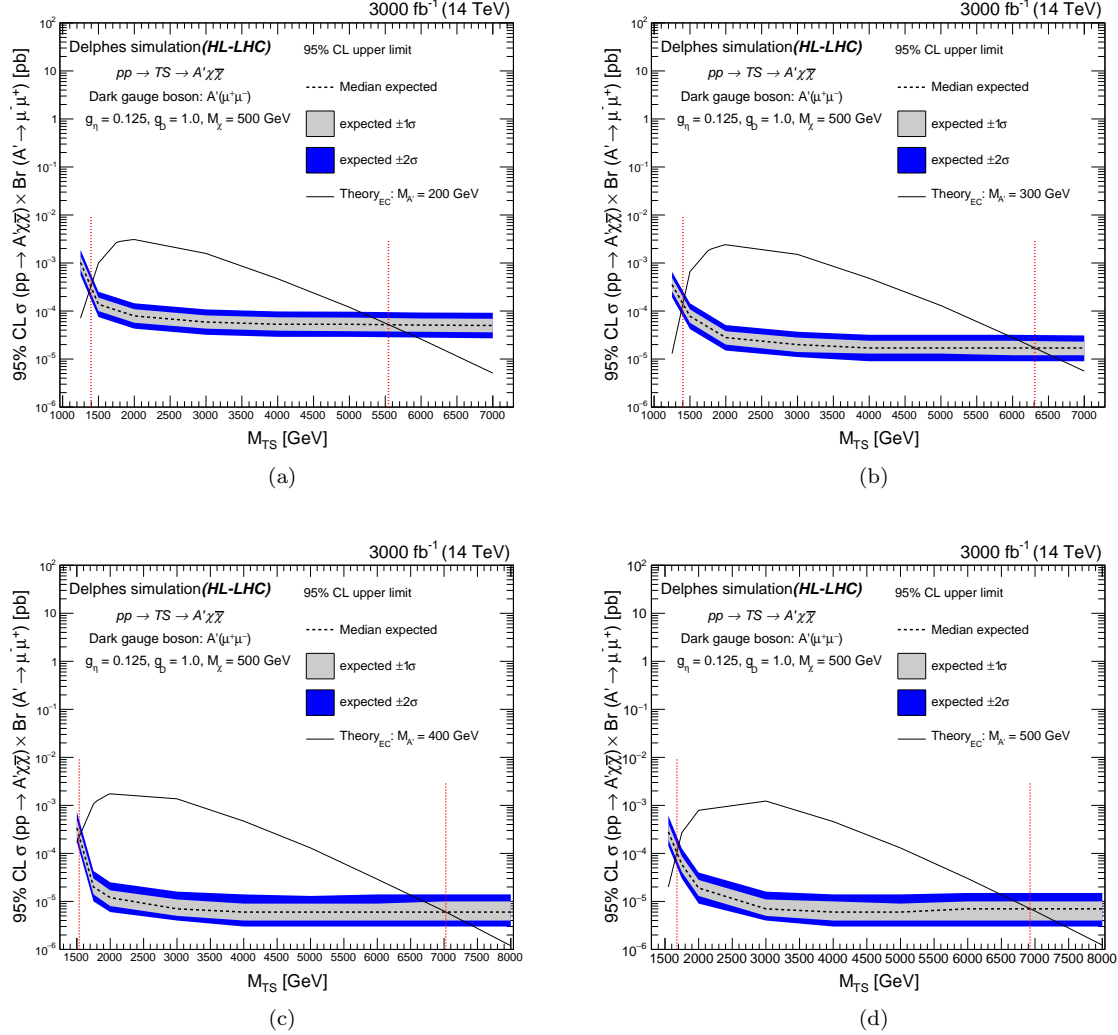


Figure 8 95% CL upper limits on the cross-section times the branching ratio (expected), as a function of the mediator's mass (M_{TS}), in the framework of the Einstein-Cartan (EC) gravity, with the muonic decay of the A' with $M_{A'} = 200$ GeV in 8(a), 300 GeV in 8(b), 400 GeV in 8(c), and 500 GeV in 8(d). The black solid curves represent the model based on Einstein-Cartan gravity at fixed dark matter mass ($M_\chi = 500$ GeV), $g_\eta = 0.125$, $g_D = 1.0$, and different values of A' mass. The vertical red dotted lines in each graph indicate the limit values.

ACKNOWLEDGMENTS

The author of this paper would like to thank Cao H. Nam, the author of [15], for his useful discussions about the theoretical models, and for sharing with us the Uni-

versal FeynRules Output (UFO) for the model that was used for the generation of the events. This paper is based on works supported by the Science, Technology, and Innovation Funding Authority (STDF) under grant number 48289.

Data Availability Statement: This manuscript has no associated data or the data will not be deposited.

- [1] F. Halzen and A. D. Martin, (1984), “Quarks And Leptons: An Introductory Course In Modern Particle Physics.” isbn: 0471887412, 9780471887416.
- [2] P. Langacker, The Physics of Heavy Z' Gauge Bosons.

- Rev. Mod. Phys., 81:1199–1228, 2008.
- [3] L. Randall and R. Sundrum, A large mass hierarchy from a small extra dimension. Phys. Rev. Lett., 83:3370–3373, 1999.

[4] Lane K. Eichten, E. and M. Peskin, New Tests for Quark and Lepton Substructure. *Phys. Rev. Lett.*, 50(11):811814, 1983.

[5] E. Eichten et al., Supercollider physics. *Rev. Mod. Phys.*, 56(4):579707, 1984.

[6] Dimopoulos S. Arkani Hamed, N. and G. Dvali, Phenomenology, Astrophysics and Cosmology of Theories with Sub-Millimeter Dimensions and TeV Scale Quantum Gravity. *Phys. Rev. D.*, 59(8), 1999.

[7] The CMS Collaboration, Search for resonant and nonresonant new phenomena in high mass dilepton final states at $\sqrt{s} = 13$ TeV. *JHEP* 07 (2021) 208.

[8] Marcelo Autran, Kevin Bauer, Tongyan Lin, and Daniel Whiteson, Searches for dark matter in events with a resonance and missing transverse energy. *Physical Review D* 92 (2015) 035007 [arXiv:1504.01386] [hep-ph].

[9] A. Gupta, R. Primulando, P. Saraswat, A new probe of dark sector dynamics at the LHC. *JHEP* 09, 079 (2015). [arXiv:1504.01385] [hep-ex].

[10] CMS Collaboration, Forward-backward asymmetry of Drell-Yan lepton pairs in pp collisions at $\sqrt{s} = 8$ TeV. *Eur. Phys. J. C* 76 (2016) 325.

[11] ATLAS Collaboration, Measurement of the angular coefficients in Z-boson events using electron and muon pairs from data taken at $\sqrt{s} = 8$ TeV with the ATLAS detector. *JHEP* 08 (2016) 159.

[12] CMS Collaboration, Measurement of the Drell-Yan forward-backward asymmetry at high dilepton masses in proton-proton collisions at $\sqrt{s} = 13$ TeV. *JHEP* 08 (2022) 063.

[13] O. Brüning and L. Rossi, The High Luminosity Large Hadron Collider: New Machine for Illuminating the Mysteries of the Universe, edited by T. Dumont and L. Rossi (2024), pp. 1-53.

[14] X. Vidal, et al., Beyond the Standard Model Physics at the HL-LHC and HE-LHC. CERN-LPCC-2018-05. arXiv:1812.07831v4 [hep-ph].

[15] Cao H. Nam, Probing dark gauge boson via Einstein-Cartan portal. *Phys. Rev. D* 105, 075015 (2022) [arXiv:2112.10446] [hep-ph].

[16] T.W. B. Kibble, Lorentz Invariance and the Gravitational Field. *Journal of Mathematical Physics.* 2 (2): 212–221 (1961).

[17] Sciama, D. W., The Physical Structure of General Relativity. *Reviews of Modern Physics.* 36 (1): 463–469 (1964-01-01).

[18] Hehl, Friedrich W.; von der Heyde, Paul; Kerlick, G. David; Nester, James M. General relativity with spin and torsion: Foundations and prospects. *Reviews of Modern Physics.* 48 (3): 393–416.

[19] Dimitri Tsoubelis, Gravitational Field of a Spin-Polarized Cylinder in the Einstein-Cartan Theory of Gravitation. *Phys. Rev. Lett.* 51, 2235 (1983).

[20] M. Shaposhnikov, A. Shkerin, I. Timiryasov, and S. Zell, Einstein-Cartan gravity, matter, and scale-invariant generalization, *J. High Energy Phys.* 10 (2020) 177.

[21] M. Shaposhnikov, A. Shkerin, I. Timiryasov, and S. Zell, Einstein-Cartan Portal to Dark Matter. *Phys. Rev. Lett.* 126, 161301 (2021).

[22] Planck Collaboration, Planck 2015 results. XIII. Cosmological parameters, *Astron. Astrophys.* 594 (2016) A13 [arXiv:1502.01589] [INSPIRE-HEP].

[23] Planck Collaboration, VI. Cosmological parameters. *A&A* 641, A6 (2020) arXiv:1807.06209 [astro-ph.CO].

[24] Craig Lage and Glennys R. Farrar, The bullet cluster is not a cosmological anomaly, *JCAP*, vol. 2015, no. 2, 038.

[25] Robert J. Scherrer and Michael S. Turner, On the relic, cosmic abundance of stable, weakly interacting massive particles, *Phys. Rev. D* 33 (1986) 1585.

[26] M. Beltran et al., “Maverick dark matter at colliders”, doi:10.1007/JHEP09(2010)037.

[27] CMS Collaboration, Dark sector searches with the CMS experiment. *Phys. Rept.* 1115 (2025) 448.

[28] ATLAS Collaboration, Exploration at the high-energy frontier: ATLAS Run 2 searches investigating the exotic jungle beyond the Standard Model. *Phys. Rep.* 1116 (2025) 301-385.

[29] Krovi AniruDF, Low Ian and Zhang Yue, Broadening dark matter searches at the LHC: mono-X versus darkonium channels. *JHEP* 10 (2018) 026 [arXiv:1807.07972] [hep-ph].

[30] CMS Collaboration, Search for new physics in final states with an energetic jet or a hadronically decaying W or Z boson and transverse momentum imbalance at $\sqrt{s} = 13$ TeV, *Phys. Rev. D* 97 (2018) 092005. [arXiv:1712.02345] [hep-ex].

[31] ATLAS Collaboration, Search for dark matter in events with a hadronically decaying vector boson and missing transverse momentum in pp collisions at $\sqrt{s} = 13$ TeV with the ATLAS detector, *JHEP* 10 (2018) 180 [arXiv:1807.11471] [hep-ex].

[32] CMS Collaboration, Search for dark matter produced in association with a leptonically decaying Z boson in proton-proton collisions at $\sqrt{s} = 13$ TeV. *Eur. Phys. J. C* 81 (2021) 13; Erratum: *Eur. Phys. J. C* 81 (2021) 333.

[33] ATLAS Collaboration, Search for associated production of a Z boson with an invisibly decaying Higgs boson or dark matter candidates at $\sqrt{s} = 13$ TeV with the ATLAS detector. *Phys. Lett. B* 829 (2022) 137066.

[34] CMS Collaboration, Search for new physics in the monophoton final state in proton-proton collisions at $\sqrt{s} = 13$ TeV, *JHEP.* 10 (2017) 073, [arXiv:1706.03794v2] [hep-ex].

[35] ATLAS Collaboration, Search for dark matter in association with an energetic photon in pp collisions at $\sqrt{s} = 13$ TeV with the ATLAS detector, *JHEP* 02 (2021) 226, [arXiv:2011.05259v2] [hep-ex].

[36] CMS Collaboration, Search for dark matter particles produced in association with a Higgs boson in proton-proton collisions at $\sqrt{s} = 13$ TeV, *JHEP* 03 (2020) 025, [arXiv:1908.01713v2] [hep-ex].

[37] ATLAS Collaboration, Search for dark matter produced in association with a Standard Model Higgs boson decaying into b-quarks using the full Run 2 dataset from the ATLAS detector, *JHEP* 11 (2021) 209, [arXiv:2108.13391v2] [hep-ex].

[38] ATLAS Collaboration, Search for dark matter in events with missing transverse momentum and a Higgs boson decaying into two photons in pp collisions at $\sqrt{s} = 13$ TeV with the ATLAS detector, *JHEP* 10 (2021) 13, [arXiv:2104.13240v2] [hep-ex].

[39] R. K. Leane, T. R. Slatyer, J. F. Beacom, and K. C. Ng, GeV-scale thermal WIMPs: Not even slightly ruled out, *Phys. Rev. D* 98 (2018), no. 2 023016, [arXiv:1805.10305].

[40] Jan Conrad and Olaf Reimer, Indirect dark matter searches in Gamma- and Cosmic Rays, *Nature Physics*, Volume 13, Issue 3, pp. 224-231 (2017).

[41] A. Boveia et al., Recommendations on presenting LHC

searches for missing transverse energy signals using simplified s-channel models of dark matter, *Phys. Dark Univ.* **27** (2020) 100365 [[arXiv:1603.04156](https://arxiv.org/abs/1603.04156)] [[INSPIRE](https://inspirehep.net/search?p=find+EPRINT+arXiv:1603.04156)].

[42] J. Collins and D. Soper, Angular distribution of dileptons in high-energy hadron collisions. *Phys. Rev. D.*, **16**(7):2219–2225, 1977.

[43] CMS Collaboration, *J. Instrum.* **3** (2008) S08004.

[44] G. L. Bayatian, *J. Phys. G* **34** (2007) CERN-LHCC-2006-021; CMS-TDR-008-2; FERMILAB-CONF-07-831-CMS.

[45] Johan Alwall, Michel Herquet, Fabio Maltoni, Olivier Mattelaer, and Tim Stelzer. *MadGraph 5 : Going Beyond*. *JHEP*, 06:128, 2011.

[46] T. Sjöstrand, S. Ask, J.R. Christiansen, R. Corke, N. Desai, P. Ilten, S. Mrenna, S. Prestel, C.O. Rasmussen, P.Z. Skands. An Introduction to PYTHIA 8.2, *Comput. Phys. Commun.* **191** (2015) 159–177, [arXiv:1410.3012](https://arxiv.org/abs/1410.3012) [hep-ph].

[47] J. de Favereau, C. Delaere, P. Demin, A. Giannmanco, V. Lemaître, A. Mertens, M. Selvaggi, DELPHES 3, A modular framework for fast simulation of a generic collider experiment, *JHEP* **1402** (2014).

[48] CMS Collaboration, Search for resonant and nonresonant new phenomena in high-mass dilepton final state at $\sqrt{s} = 13$ TeV, *JHEP* **07** (2021) 208 [[arXiv:2103.02708v2](https://arxiv.org/abs/2103.02708v2)] [hep-ex].

[49] CMS Collaboration, Search for Supersymmetry in pp Collisions at 7 TeV in Events with Jets and Missing Transverse Energy. *Physics Letters B*, Volume 698, Issue 3, 11 April 2011, Pages 196–218.

[50] P. Osland, A. A. Pankov, A. V. Tsytrinov and N. Paver, Spin identification of the Randall-Sundrum resonance in lepton-pair production at the CERN LHC, *PHYSICAL REVIEW D* **78**, 035008 (2008).

[51] A. L. Read, Presentation of search results: the CLs technique, *J. Phys. G: Nucl. Part. Phys.* **28** (2002) 2693, doi:10.1088/0954-3899/28/10/313.

[52] T. Junk, Confidence level computation for combining searches with small statistics, *Nuclear Instruments and Methods in Physics Research Section A: Accelerators, Spectrometers, Detectors and Associated Equipment*, Volume 434, Issues 2–3, 1999, Pages 435–443, ISSN 0168-9002, [https://doi.org/10.1016/S0168-9002\(99\)00498-2](https://doi.org/10.1016/S0168-9002(99)00498-2).

[53] G. Cowan et al., Asymptotic formulae for likelihood-based tests of new physics, *Eur. Phys. J. C* **71** (2011), p. 1554, doi: 10.1140/epjc/s10052-011-1554-0, [arXiv: 1007.1727](https://arxiv.org/abs/1007.1727) [physics.data-an], Erratum: *Eur. Phys. J. C* **73** (2013) 2501.